

Tracking solvent and protein movement during CO₂ release in carbonic anhydrase II crystals

Chae Un Kim^{a,b,1}, Hyojin Song^c, Balendu Sankara Avvaru^d, Sol M. Gruner^{a,e}, SangYoun Park^{c,1}, and Robert McKenna^{d,1}

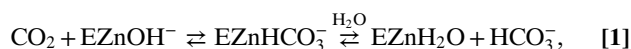
^aCornell High Energy Synchrotron Source, Cornell University, Ithaca, NY 14853; ^bDepartment of Physics, Ulsan National Institute of Science and Technology, Ulsan 44919, Republic of Korea; ^cSchool of Systems Biomedical Science, Soongsil University, Seoul 06978, Republic of Korea; ^dDepartment of Biochemistry and Molecular Biology, College of Medicine, University of Florida, Gainesville, FL 32610; and ^eDepartment of Physics, Cornell University, Ithaca, NY 14853

Edited by Keith Moffat, The University of Chicago, Chicago, IL, and accepted by the Editorial Board March 22, 2016 (received for review October 20, 2015)

Carbonic anhydrases are mostly zinc metalloenzymes that catalyze the reversible hydration/dehydration of CO₂/HCO₃⁻. Previously, the X-ray crystal structures of CO₂-bound holo (zinc-bound) and apo (zinc-free) human carbonic anhydrase IIs (hCA IIs) were captured at high resolution. Here, we present sequential timeframe structures of holo- [T = 0 s (CO₂-bound), 50 s, 3 min, 10 min, 25 min, and 1 h] and apo-hCA IIs [T = 0 s, 50 s, 3 min, and 10 min] during the “slow” release of CO₂. Two active site waters, W_{DW} (deep water) and W_{DW'} (this study), replace the vacated space created on CO₂ release, and another water, W_I (intermediate water), is seen to translocate to the proton wire position W1. In addition, on the rim of the active site pocket, a water W2' (this study), in close proximity to residue His64 and W2, gradually exits the active site, whereas His64 concurrently rotates from pointing away (“out”) to pointing toward (“in”) active site rotameric conformation. This study provides for the first time, to our knowledge, structural “snapshots” of hCA II intermediate states during the formation of the His64-mediated proton wire that is induced as CO₂ is released. Comparison of the holo- and apo-hCA II structures shows that the solvent network rearrangements require the presence of the zinc ion.

carbonic anhydrase II | CO₂ release | intermediate states | high-pressure cryocooling

Carbonic anhydrases (CAs) are mostly zinc metalloenzymes that catalyze the reversible hydration/dehydration of CO₂/HCO₃⁻ (general reviews are in refs. 1–5). In the hydration direction, the first step of catalysis is the conversion of CO₂ into bicarbonate through the nucleophilic attack of the reactive Zn-bound hydroxide, and the resultant bicarbonate is subsequently displaced from the zinc by a water molecule (expression 1) (6). The second step of catalysis is the transfer of a proton from the Zn-bound water to bulk solvent for the regeneration of the Zn-bound hydroxide. The general base for proton transfer (PT), B, can be either a proton acceptor in solution (water) or a residue (His64) in the enzyme (expression 2):



and



There are 16 mammalian CAs, of which human carbonic anhydrase II (hCA II) is the best studied because of its role in many physiological processes (4, 5, 7). hCA II, like all mammalian CAs, belongs to the α -class CAs based on their structural homology (8). The active site zinc is located deep within a 15-Å-deep cleft and tetrahedrally coordinated by three histidines (His94, His96, and His119) and a Zn-bound solvent (W_{Zn}) (2). The active site cavity is further subdivided into two distinct sides of hydrophobic (consisting of Val121, Val143, Leu198, Thr199-CH₃, Val207, and Trp209) and hydrophilic (consisting of

Tyr7, Asn62, His64, Asn67, Thr199-O_{γ1}, and Thr200-O_{γ1}) residues. The hydrophobic side sequesters and orients the CO₂ for nucleophilic attack by the Zn-bound hydroxide (expression 1 and Fig. 1) (9).

The hydrophilic side of the active site coordinates a hydrogen-bonded solvent network (W1, W2, W3a, and W3b) that connects the Zn-bound solvent to His64 and is believed to be involved in the transfer of a proton from the Zn-bound water to bulk solvent for the regeneration of the Zn-bound hydroxide (expression 2 and Fig. 1) (10, 11). Thr199 forms a hydrogen bond to the W_{Zn} that, in turn, is hydrogen-bonded to W1. W1 is further stabilized by Thr200 and the next solvent in the chain, W2. The solvent network then branches, because W2 is hydrogen-bonded to both W3a and W3b. W3a is further coordinated by the hydroxyl group of Tyr7, whereas W3b is stabilized by Asn62 and Asn67 (12, 13). This solvent network has been previously shown to be conserved over a broad pH range (pH 5.0–10.0) and localizes W2, W3a, and W3b all in close proximity to the side chain of His64 when orientated in the “in” conformation (pointing toward the active site) (9, 11, 14, 15).

The structural examination of hCA II at near atomic resolution revealed that the solvent molecule W2 (the only ordered solvent molecule in the active site stabilized exclusively by other solvent molecules) is trigonally coordinated with equal distance (2.75 ± 0.02 Å) by W1, W3a, and W3b (16). Within this cluster of

Significance

Carbonic anhydrases catalyze the fast interconversion of carbon dioxide and water into bicarbonate and proton. In this study, we use the method of high-pressure cryocooling to capture the gaseous carbon dioxide in crystals of carbonic anhydrase and follow the sequential structure changes as the carbon dioxide is released. These “snapshots” enable us to “slow down” and visualize the water and protein motions that form a “proton wire” as the carbon dioxide exits the enzyme’s active site. This study provides an understanding of the importance of water rearrangements within an enzyme-active site and further suggests that such a method could be generally applied to other protein-mediated reactions that use gaseous molecules.

Author contributions: C.U.K. designed research; C.U.K. and B.S.A. performed research; C.U.K. and S.P. analyzed data; and C.U.K., H.S., B.S.A., S.M.G., S.P., and R.M. wrote the paper.

The authors declare no conflict of interest.

This article is a PNAS Direct Submission. K.M. is a guest editor invited by the Editorial Board.

Data deposition: The crystallography, atomic coordinates, and structure factors have been deposited in the Protein Data Bank, www.pdb.org (PDB ID codes 5DS1, 5DSJ, 5DSK, 5DSL, 5DSM, 5DSN, 5DSO, 5DSP, 5DSQ, and 5DSR).

¹To whom correspondence may be addressed. Email: cukim@unist.ac.kr, psy@ssu.ac.kr, or rmckenna@ufl.edu.

This article contains supporting information online at www.pnas.org/lookup/suppl/doi:10.1073/pnas.1520786113/-DCSupplemental.

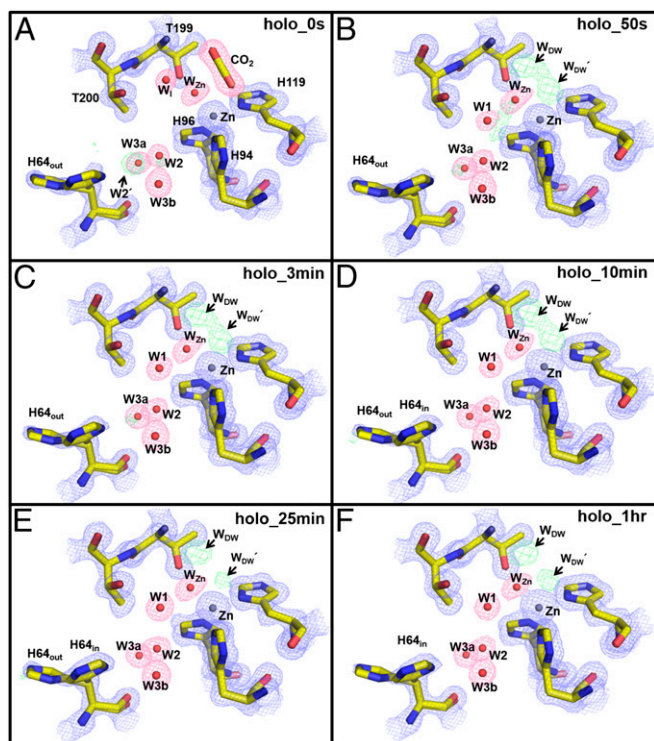


Fig. 1. Holo-hCA II active site solvent structure during CO₂ release: (A) 0 s, (B) 50 s, (C) 3 min, (D) 10 min, (E) 25 min, and (F) 1 h. Electron density $2F_o - F_c$ (blue) and $F_o - F_c$ (green) maps are contoured at 1.5σ and 5.0σ , respectively. The $2F_o - F_c$ maps for waters and CO₂ are highlighted in pink for clarity. Note the omitted density of W2' (in A) and the appearance of W_{DW} and W_{DW}' (CO₂-substituting solvent in E and F). Also, W₁ is only observed in the CO₂-bound hCA II (in A) as opposed to W₁ (in B–F). Solvent and amino acids are as labeled.

solvent molecules, only W₂ is in the plane of the imidazole ring of His64 and within hydrogen-bonding distance of His64. It is thought that, when in an in conformation, His64 and the Zn-bound water with pK_a values of ~7 facilitate the proton shuttling process (Fig. 1) (17, 18).

Previously, the crystallographic capture of CO₂ in the active site of hCA II was achieved by high-pressure cryocooling of crystals (19, 20). The visualized CO₂ was bound in the hydrophobic one-half of the conical active site in identical orientations in both holo and apo crystal structures, indicating that stabilization of the substrate is independent of the active site zinc ion as previously hypothesized, and it seems to be solely dependent on the hydrophobicity of the binding pocket (21). In the absence of CO₂ substrate, an additional active site solvent molecule termed deep water (W_{DW}) resides in the hydrophobic pocket in unbound crystal structures. In crystal structures with bound CO₂ substrate, the stabilized substrate was found to displace the W_{DW} from its position; the W_{DW} displacement by CO₂ is most likely a consequence of the higher propensity of CO₂ for the hydrophobic pocket than water (20).

In this study, we have further developed this method to examine intermediate states of hCA II during the gradual release of CO₂. We incubated the CO₂-bound holo- and apo-hCA II crystals at room temperature (RT) for various incubation periods and flash-cooled them before subjecting them to X-ray diffraction data collection. Here, we describe various structural changes in the active site solvent network and the in and “out” conformations of His64 (the proton shuttle residue) as the CO₂ gas gradually escapes the hCA II crystals over a time course of 1 h. Contrasting these structures with CO₂-bound hCA II structure

has revealed important features in the active site and provided additional insight into the enzymatic mechanism of hCA II.

Results and Discussion

CO₂ Release: Active Site (CO₂/W_{Zn}/W_{DW}/W_{DW}'/W₁/W₁) Holo-hCA II. To analyze the dynamics of solvent and track amino acid conformational changes during CO₂ release in the active site, intermediate states of holo-hCA II were prepared by incubating the CO₂ pressurized holo-hCA II crystals at RT for time intervals [0 s (no incubation), 50 s, 3 min, 10 min, 25 min, and 1 h] and flash-cooling them to 100 K before X-ray diffraction data collection. The crystal incubation times at RT (from 50 s to 1 h) were carefully chosen to gradually drop the partial pressure of CO₂ in the holo-hCA II crystals. In this way, the holo-hCA II states were gradually shifted from the CO₂-bound state to the CO₂-free state (*SI Materials and Methods*).

The CO₂-bound holo-hCA II (0 s; no incubation) was compared with the previously reported structures of CO₂-bound holo-hCA II [Protein Data Bank (PDB) ID code 3D92 (20); all atom rmsd = 0.30 Å] and CO₂-free holo-hCA II [PDB ID codes 3KS3 (18) and 2ILI (22)] and as expected, showed that the starting CO₂-bound state was identical to that reported in 3D92. The positions of amino acids forming the active site around the zinc and the W_{Zn} were also identical in the CO₂-free holo-hCA IIs with all atom rmsd = 0.43 Å (3KS3), 0.53 Å (2ILI), and 0.62 Å (3D93) (Fig. S1).

The CO₂-bound holo-hCA II crystals incubated at RT (50 s, 3 min, 10 min, and 25 min) showed a gradual deterioration of electron density where the CO₂ was previously bound (i.e., at 0 s), with negligible changes in the surrounding zinc and coordinating histidines (His94, His96, and His119). The electron density changes form from bound CO₂ (0 s) to two connected lobes (50 s, 3 min, and 10 min) to two separate and distinct spherical densities (25 min and 1 h) (Fig. 1). The observed change in electron density suggests that, as CO₂ leaves the active site, the void space is replaced by two water molecules. Interestingly, the density profile does not indicate the formation of bicarbonate; instead, it indicates the slow removal of CO₂, suggesting that the pH of the crystal is too acidic for the hydration reaction, indicative of a Zn-bound water. In the two lobes of electron densities, the one nearest Thr199 represents deep water (W_{DW}), which is also well-ordered in the CO₂-free holo-hCA II (Fig. S1 C and D). The second lobe represents a water molecule that was also previously observed in the CO₂-free holo-hCA II (3KS3) (Fig. S1C) (18). We refer to this water as W_{DW}' . In all of the incubation series, W_{DW} and W_{DW}' that replace CO₂ are observed nearer to the W_{Zn} than CO₂. However, the distance between W_{DW} and W_{DW}' (~2.1 Å) indicates that the two waters can only be partially occupied. Of note, the distance between the zinc and W_{DW}' (~2.6 Å) is significantly longer than the distances between zinc and its coordinating W_{Zn}, His94, His96, and His119, which have distances of ~2.0 Å (Fig. 2).

Previously, the CO₂-bound holo-hCA II structure (PDB ID code 3D92) revealed a newly observed water termed water intermediate, W₁, located near Thr199, which had not been observed in other CO₂-free hCA II structures (Fig. S1) (20). The density for W₁ in our holo-hCA II T = 0 s structure confirms that W₁ is present when CO₂-bound (Fig. 1). The distance between W₁ and W₂ is 4.8 Å, which suggests that the hydrogen-bonded solvent network for the PT breaks as CO₂ binds in the active site (Fig. 2). However, the W₁ has shifted or was left in the active site for all subsequent incubation time points, coinciding with the restoration of W₁ (Figs. 1 and 2). The data indicate that the hydrogen bonding in the active site water cluster of holo-hCA II is restored on the release of CO₂, establishing a molecular pathway for shuttling protons between the bulk solvent and the catalytic center.

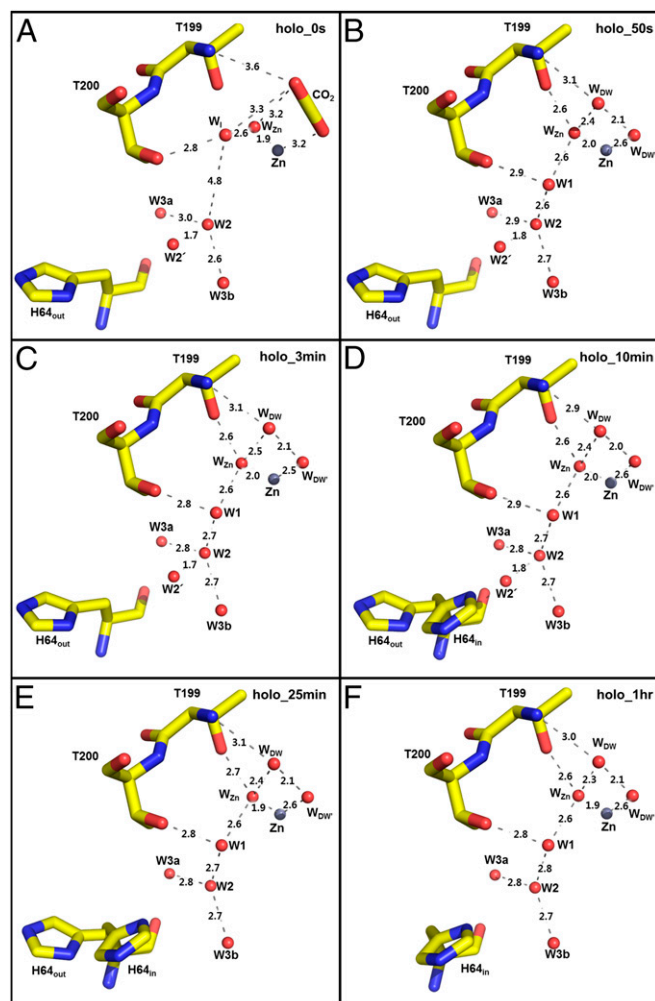


Fig. 2. Holo-hCA II active site solvent network during CO₂ release: (A) 0 s, (B) 50 s, (C) 3 min, (D) 10 min, (E) 25 min, and (F) 1 h. Hydrogen bond distances (angstrom) are depicted as dotted lines. The major conformation of His64 is in the out positions for 0 s, 50 s, and 3 min (A–C) and the in position at 1 h (F). Solvent and amino acids are as labeled.

His64 and the W1/W2'/W2/W3a/W3b Water Network in Holo-hCA II.

The proton shuttling residue, His64, has previously been shown to exhibit two configurations, pointing toward (in) and pointing away (out) from the active site, depending on the C α –C β bond rotation (9, 23). Also, His64 and the solvent network (W1, W2, W3a, and W3b) have been proposed to be critical for the PT (expression 1) and the rate-limiting step in holo-hCA II turnover (11). During the CO₂ time-released experiments, the His64 configuration in the holo-hCA II series gradually transitions from the out to the in position (Fig. 3). Previously, the pH effect on the His64 configurations was suggested where His64 favors the out position at low pH and the in position at high pH (9). Accordingly, in this study, the CO₂ pressurization would lower the pH of the holo-hCA II crystals to less than pH 6 and result in His64 to occupy the out position (20). As the CO₂ in the crystal is gradually released, restoration of a higher pH would shift the His64 conformation into an in position, with it fully occupying the in conformer at 1 h (Fig. 3).

In addition, electron density likely representing a water, W2', between His64 and W2 in the holo-hCA II series was observed (Figs. 1*A* and 3*A* and Fig. S1). This water density gradually dissipates with time, is gone after 25 min, a consequence of CO₂ release, and leaves a vacant space for His64 to

occupy the in conformation (Figs. 1 and 3). In the previous CO₂-bound holo-hCA II structure [PDB ID code 3D92 (20)], a glycerol molecule was modeled in this region (Fig. S1*B*). In this study, these electron densities near His64 were built as the water molecules (W2', W2, and W3b) and part of the solvent network (Fig. 3).

The observation of W2' between W2 and His64 gradually disappearing in the holo-hCA II time series suggests that W2' is an alternate position of W2 (the 1.7-Å distance between W2' and W2). The fact that the side chain of His64 moves from an out to an in position coincides with the loss of W2', suggesting that His64 out position permits both water positions W2 and W2', whereas His64 in position crystallographically favors a water position at W2 because of steric hindrance. However, considering the dynamical in and out movement of His64, the water W2' can be sufficiently close enough to form a hydrogen bond to His64 when it moves inwards. This observation provides evidence for the role of W2 in the PT. Previously, it was unclear which water molecule among W2, W3a, and W3b that surround His64 actually performs the transfer of a proton to His64, because they were always highly ordered but all too far (3.3–3.8 Å) for His64 to form a hydrogen bond. These data suggest that W2 and W2' are likely the bridging waters to the nitrogen of His64, forming the proton wire. Also, contrary to the observed dynamics of His64 and W2/W2', it is interesting to note that the distances between W1, W2, W3a, and W3b are invariant in the holo-hCA II incubation series (Fig. 2).

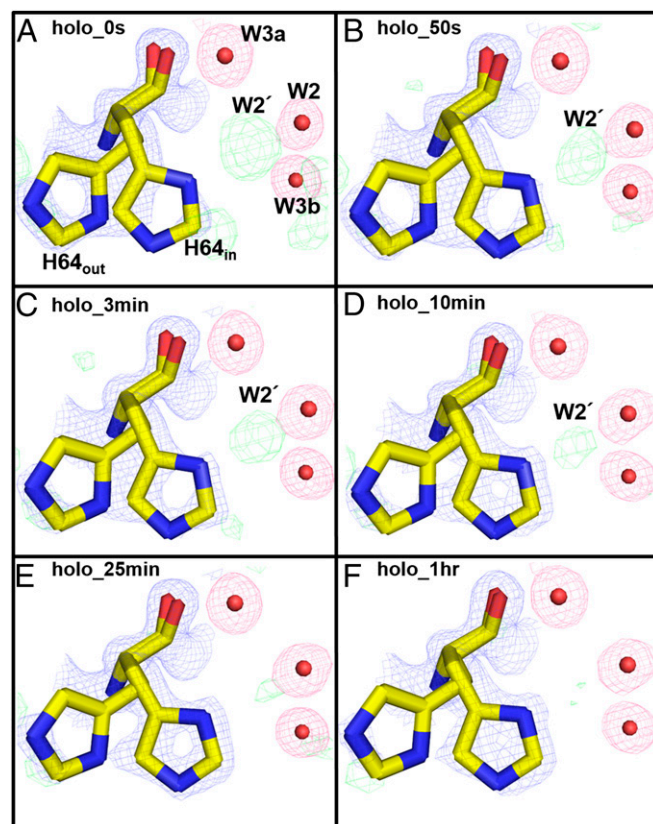


Fig. 3. Holo-hCA II rotameric states of His64: (A) 0 s, (B) 50 s, (C) 3 min, (D) 10 min, (E) 25 min, and (F) 1 h. Electron density $2F_o-F_c$ (blue) and F_o-F_c (green) maps are contoured at 1.5 σ and 3.0 σ , respectively. The $2F_o-F_c$ maps for waters are highlighted in pink for clarity. On CO₂ release and gradual dissipation of W2', the His64 side chain shifts from the out to the in position. Solvent and amino acids are as labeled.

It should also be noted that the dynamics of His64 have also been coupled to small molecules that can activate the enzyme catalytic rate, termed “activators,” which bind in the vicinity of His64 and are distinguished from inhibitors, because they bind away from the substrate binding site (24). These transient enzyme activator complexes significantly enhance catalysis by speeding up the rate-limiting PT step through an intramolecular process (25). The initial X-ray structures of enzyme activator complexes were mostly reported as in conformers of His64 (26–28); however, subsequently, out conformation of His64 has also been observed (29). These observations show how dynamic the active site is and why understanding the motion of solvent in the active site is critical to fully understanding the enzyme’s mechanism.

CO₂ Release: Active Site (CO₂/W_{Zn}/W_{DW}/W_{DW}’/W₁/W₁) Apo-hCA II. In a similar set of experiments, crystals of apo-hCA II (zinc removed) were also CO₂-pressurized, incubated at RT at time intervals [0 s (no incubation), 40 s, 3 min, and 10 min], and flash-cooled to 100 K before diffraction experiment (*SI Materials and Methods*). Structural comparison of the apo-hCA II (0 s; no incubation) with the previously determined CO₂-bound apo-hCA II structure [PDB ID code 3D93 (20)] was shown to be identical (all atom rmsd = 0.58 Å) (Fig. S2).

Analysis of the apo-hCA II four incubation time points (0 s, 40 s, 3 min, and 10 min) showed gradual changes of electron density near the CO₂ binding site with negligible changes in the active site histidines (His94, His96, and His119) (Fig. 4). As seen with the holo-hCA II structures, the electron density profile shifted inward toward the W_{Zn}, forming two distinct spheres (W_{DW} and W_{DW}’). However, the continuous lobes in the apo-hCA II separate into the two isolated W_{DW} and W_{DW}’ between 3 and 10 min; it happened at a shorter timescale compared with that of the holo-hCA II, which happened between 10 and 25 min. As observed in the holo-hCA II, the distance between W_{DW} and W_{DW}’ was short, suggesting that the two waters can only be partially occupied (Fig. 5). Also, in the apo-hCA II, the electron density representing W_{DW}’ is diminished at 10 min, which is in contrast to the consistent

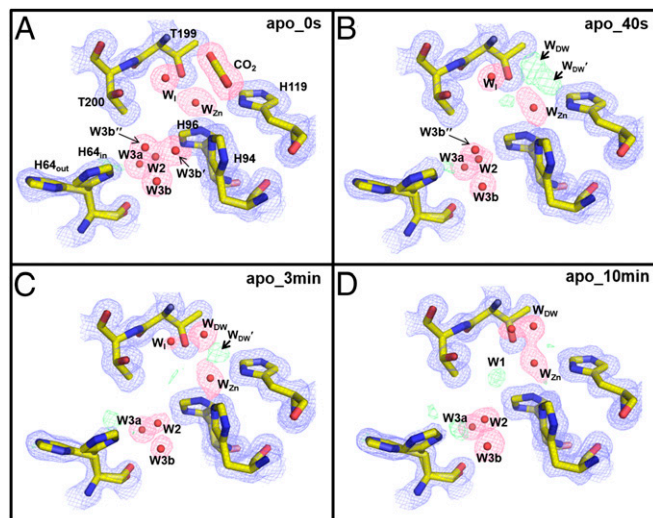


Fig. 4. Apo-hCA II active site solvent structure during CO₂ release: (A) 0 s, (B) 50 s, (C) 3 min, and (D) 10 min. Electron density $2F_o - F_c$ (blue) and $F_o - F_c$ (green) maps are contoured at 1.5σ and 5.0σ , respectively. The $2F_o - F_c$ maps for waters and CO₂ are highlighted in pink for clarity. Note that the two solvent molecules in close proximity to W3b are observed only at 0 s (A). As was observed for the holo-hCA II, W_{DW} and W_{DW}’ substitute the released CO₂. Solvent and amino acids are as labeled.

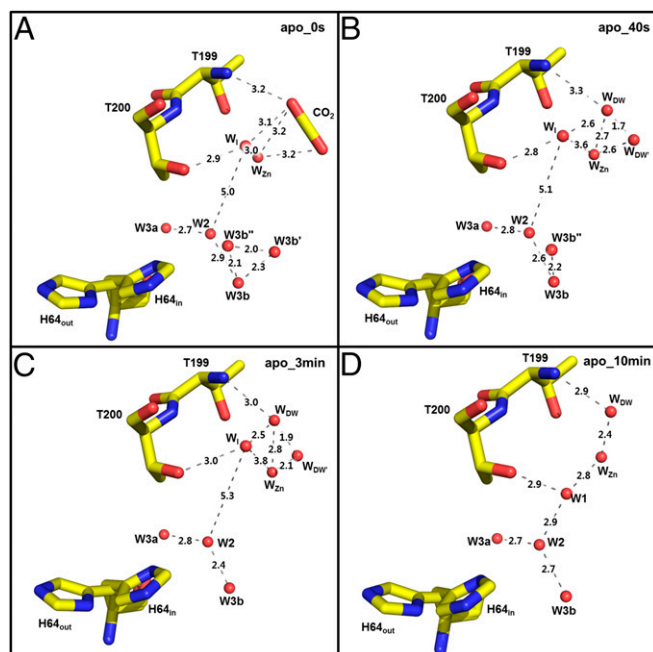


Fig. 5. Apo-hCA II active site solvent network during CO₂ release: (A) 0 s, (B) 50 s, (C) 3 min, and (D) 10 min. Hydrogen bond distances (angstrom) are depicted as dotted lines.

W_{DW}’ density in the holo-hCA II. These observations may be explained in the following way. The connected density for W_{DW} and W_{DW}’ indicates that CO₂ is still partially occupied along with W_{DW} and W_{DW}’. In the apo-hCA II, as CO₂ diffuses out, the electron density of CO₂ gradually decreases, and its density is simply replaced by W_{DW} and W_{DW}’. However, as CO₂ diffuses out in the holo-hCA II, the reverse reaction of holo-hCA II (expression 1) converts water-resolved bicarbonate to CO₂, which may be maintaining CO₂ partial occupancy in the active site for a longer time. The presence of the zinc in the holo-hCA II seems to make W_{DW}’ more stable, which remains unclear.

As observed with the holo-hCA II at 0 s, W₁ is present in the active site when CO₂ is bound (Figs. 4 and 5). However, in contrast to W₁ leaving the active site and W₁ appearing relatively rapidly (before 50 s) in the holo-hCA II, W₁ still exists in the apo-hCA II at 3 min and only leaves when W₁ appears at 10 min. In the apo-hCA II, the W₁ to W₁ shift takes place “more slowly” in contrast to the “faster solvent” changes for W_{DW} and W_{DW}’. In both holo-hCA II and apo-hCA II, W₁ is stabilized by making hydrogen bonds with Thr200 and W₂ water. Interestingly, the electron density of W₂ is significantly weaker in the early apo-hCA II incubation series than in the holo-hCA II incubation series (see below). This weak W₂ suggests that W₁ position is relatively destabilized in the apo-hCA II, which may explain why the W₁ to W₁ shift is slower in apo-hCA II than in holo-hCA II.

His64 and the W₁/W₂/W₂’/W_{3a}/W_{3b} Water Network in Apo-hCA II. In the apo-hCA II incubation series, the solvent network of W₂’ and W₂ differs from that of holo-hCA II. In the apo-hCA II at 0 s structure, there is no observable density for W₂’ and only faint density for W₂ (Fig. 6 and Fig. S2). Also, the two waters (termed as W_{3b}’ and W_{3b}’’) unobserved in holo-hCA II near W_{3b} at 0 s were observed in the counterpart apo-hCA II at 0 s (Figs. 4 and 5). W_{3b}’ was also observed in the previous CO₂-bound apo-hCA II structure (PDB ID code 3D93). The presence of the new waters W_{3b}’ and W_{3b}’’ in the apo-hCA II

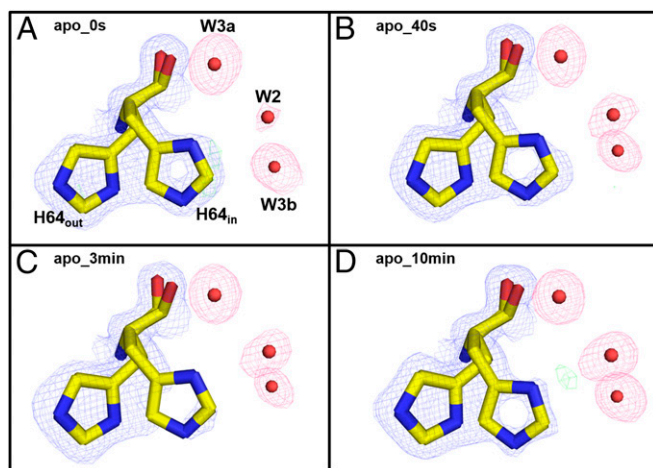


Fig. 6. Conformation of His64 in apo-hCA II: (A) 0 s, (B) 50 s, (C) 3 min, and (D) 10 min. The $2F_o - F_c$ (blue) and $F_o - F_c$ (green) electron density maps are contoured at 1.0σ and 5.0σ , respectively. The $2F_o - F_c$ maps for waters are highlighted in pink for clarity. There is no evidence of a preferable His64 position (in vs. out) or $W2'$ (except maybe in D).

reflects the altered electrostatic environment of the active site in the absence of Zn at the saturation of CO_2 under high pressure. They gradually disappear over time, and the passive escape of CO_2 gas from the active site most likely perturbs their stability. The most notable difference is the lack of any conformational changes in the apo-hCA II incubation series of His64 during CO_2 release, unlike holo-hCA II (Figs. 3 and 6). These observations reiterate the importance of the zinc for not only its catalytic role but also, the proper rearrangement of the solvent network, which is necessary for efficient PT. In the absence of PT in the apo-hCA II, the side chain of His64 is mostly locked in the out conformation, whereas the holo-hCA II with an intact PT displays dual occupancy for the side chain of His64. It appears that the orientation of the side chain of His64 is effectively controlled by the electrostatic influence of the Zn. The pK_a values of His64 and Zn solvent titrate to 7.2 and 6.8, respectively, and the pH profile for enzymatic activity fits to a single ionization. Although the ordered water molecules appear in nearly identical coordinates in both apo- and holo-hCA II, the apo-hCA II does not carry a low-barrier hydrogen bond (LBHB) that exists between Zn solvent and W_{DW} , which is a significant contributor toward catalysis. The enthalpy of formation of LBHB is nearly fourfold higher than the hydrogen bonds typical of water molecules, and its formation lowers the pK_a and enhances the protolysis of the Zn solvent. The energy released and absorbed during the formation and cleavage of the LBHB during each cycle of catalysis likely influences the side chain dynamics of His64 and the movement of $W2$ to $W2'$. Lack of this LBHB may be the reason for not observing $W2'$ and His64 side chain dynamics in the apo-hCA II. Additional research is needed to clearly understand the role of zinc for the observed solvent rearrangements, solvent dynamics, and His64 movements in the holo- and apo-hCA II.

Secondary CO_2 Binding Site Near Phe226. Previously, a secondary CO_2 binding site was reported in the structures of CO_2 -bound holo- and apo-hCA II [PDB ID codes 3D92 and 3D93 (20)]. Similarly, in holo- and apo-hCA II 0 s (no incubation), this secondary CO_2 is presently located in a hydrophobic pocket near Phe226 (Figs. S3 and S4). In the holo-hCA II incubation series, by 50 s, the CO_2 seems dissipated, and the Phe226 side chain is rotated back to the position observed in the CO_2 -free state of hCA II (Fig. S3). However, for the apo-hCA II, at the 40-s time

point, the electron density for the CO_2 faintly existed, and at the 3-min point, it had gone (Fig. S4). It is still unclear whether the secondary binding/release of the substrate CO_2 functionally affects the catalytic function of the enzyme, and this phenomenon needs additional investigation.

Conclusions

Presented here are intermediate structural states of holo- and apo-hCA II observed during CO_2 release. The data show that the active site structure, although thought to be rigid, undergoes significant solvent rearrangements that are orchestrated with conformational rotamer changes of the proton shuttling residue His64. For instance, an alternate water position $W2'$ exists, forming the solvent network to His64 in the out position, whereas CO_2 is bound in the holo-hCA II; however, on CO_2 release, $W2'$ dissipates, and His64 subsequently moves from an out to the in rotameric position. The His64 out to in movement as well as $W2'$ are not being observed in the CO_2 -bound apo-hCA II structures. Also, two waters, W_{DW} and W_{DW}' , replace the vacant space created during CO_2 release in both the holo- and apo-hCA II. On CO_2 release, the CO_2 -substituted W_{DW} seems to influence and reposition $W1$ to the $W1$ position, forming the ordered proton wire. This $W1$ to $W1$ transition occurs on a longer timescale in the apo-hCA II. These results provide a near atomic view of structural snapshots of hCA II during CO_2 release and insight into the structural role of the zinc in coordinating the water network. These results also provide hints for the solvent rearrangements that occur as the zinc-bound hydroxide–water transition occurs and the mechanism of PT through the solvent network rearrangement in the hCA II as the CO_2 leaves the crystal and the pH reequilibrates from <6 to neutrality (30). Additional molecular dynamic calculations given these “static structural time points” may give more details on the flowing motion of the solvent in the active site (31, 32). This study also shows technical methods that may be applicable to other enzymes that bind and react to low-molecular weight substrates, such as CO_2 and NO_2 .

Materials and Methods

hCA II protein was expressed, purified, and crystallized as described previously (22, 33–35). The CO_2 entrapment inside hCA II crystals was carried out by cryocooling crystals under CO_2 pressure of 15 atm (19, 20). Before CO_2 pressurization, the hCA II crystals were coated with a mineral oil as a CO_2 buffering medium (36). The intermediate states during CO_2 release were captured by incubating the CO_2 -bound crystals into a mineral oil at RT for various periods over 1 h and then, flash-cooling them back to 100 K. The crystal incubation time (from ~1 min to 1 h) was carefully chosen to gradually drop the partial pressure of CO_2 in the hCA II crystals. In this way, the hCA II intermediate states equilibrated at different CO_2 partial pressures could be captured. Note that the experimental crystal incubation timescale indicates the timescale that CO_2 diffuses out of the hCA II crystals rather than the much faster catalytic reaction timescale of hCA II. The X-ray diffraction data were collected at the Cornell High Energy Synchrotron Source, and the data were processed and refined as described previously (20). For each X-ray dataset, a fresh hCA II crystal was prepared as described above, and a single complete X-ray diffraction dataset was collected with an estimated absorbed X-ray dose of 3×10^6 Gy. It was checked that X-ray dose up to 10^7 Gy does not induce any noticeable changes in the hCA II active site. Details on the experimental procedures and crystallographic refinement statistics can be found in *SI Materials and Methods* and *Tables S1* and *S2*.

ACKNOWLEDGMENTS. The authors thank the staff at the Cornell High Energy Synchrotron Source (CHESS) and the Macromolecular Diffraction at CHESS (MacCHESS) for their support and beam time and Jin Kyun Kim for assistance in manuscript preparation. This work was funded, in part, by NIH Grant GM25154. The CHESS is supported by the NSF and the NIH/NIGMS under NSF Award DMR-1332208, and MacCHESS is supported by NIH/NIGMS Award GM-103485. This research was also supported by the Basic Science Program through the National Research Foundation of Korea funded by Ministry of Science, ICT, and Future Planning Grants 2014R1A2A1A11051254 (to C.U.K.) and 2013R1A1A2005276 (to S.P.).

1. Davenport HW (1984) The early days of research on carbonic anhydrase. *Ann N Y Acad Sci* 429:4–9.
2. Christianson DW, Fierke CA (1996) Carbonic anhydrase: Evolution of the zinc binding site by nature and by design. *Acc Chem Res* 29(7):331–339.
3. Chegwidden WR, Carter ND, Edwards YH (2000) *The Carbonic Anhydrases: New Horizons* (Birkhauser, Basel).
4. Frost SC, McKenna R (2014) *Carbonic Anhydrase: Mechanism, Regulation, Links to Disease, and Industrial Applications* (Springer, Dordrecht, The Netherlands).
5. Supuran CT, de Simone G (2015) *Carbonic Anhydrases as Biocatalysts: From Theory to Medical and Industrial Applications* (Elsevier, Berlin).
6. Silverman DN, Lindskog S (1988) The catalytic mechanism of carbonic anhydrase: Implications of a rate-limiting protolysis of water. *Acc Chem Res* 21(1):30–36.
7. Krishnamurthy VM, et al. (2008) Carbonic anhydrase as a model for biophysical and physical-organic studies of proteins and protein-ligand binding. *Chem Rev* 108(3): 946–1051.
8. Hewett-Emmett D, Tashian RE (1996) Functional diversity, conservation, and convergence in the evolution of the alpha-, beta-, and gamma-carbonic anhydrase gene families. *Mol Phylogenet Evol* 5(1):50–77.
9. Fisher Z, et al. (2005) Structural and kinetic characterization of active-site histidine as a proton shuttle in catalysis by human carbonic anhydrase II. *Biochemistry* 44(4): 1097–1105.
10. Tu CK, Silverman DN, Forsman C, Jonsson BH, Lindskog S (1989) Role of histidine 64 in the catalytic mechanism of human carbonic anhydrase II studied with a site-specific mutant. *Biochemistry* 28(19):7913–7918.
11. Silverman DN, McKenna R (2007) Solvent-mediated proton transfer in catalysis by carbonic anhydrase. *Acc Chem Res* 40(8):669–675.
12. Fisher SZ, et al. (2007) Speeding up proton transfer in a fast enzyme: Kinetic and crystallographic studies on the effect of hydrophobic amino acid substitutions in the active site of human carbonic anhydrase II. *Biochemistry* 46(12):3803–3813.
13. Zheng J, Avvaru BS, Tu C, McKenna R, Silverman DN (2008) Role of hydrophilic residues in proton transfer during catalysis by human carbonic anhydrase II. *Biochemistry* 47(46):12028–12036.
14. Christianson DW (1991) Unexpected pH-dependent conformation of His-64, the proton shuttle of carbonic anhydrase-II. *J Am Chem Soc* 113(25):9455–9458.
15. Steiner H, Jonsson BH, Lindskog S (1975) The catalytic mechanism of carbonic anhydrase. Hydrogen-isotope effects on the kinetic parameters of the human C isoenzyme. *Eur J Biochem* 59(1):253–259.
16. Cui Q, Karplus M (2003) Is a “proton wire” concerted or stepwise? A model study of proton transfer in carbonic anhydrase. *J Phys Chem B* 107(4):1071–1078.
17. Lindskog S (1997) Structure and mechanism of carbonic anhydrase. *Pharmacol Ther* 74(1):1–20.
18. Avvaru BS, et al. (2010) A short, strong hydrogen bond in the active site of human carbonic anhydrase II. *Biochemistry* 49(2):249–251.
19. Kim CU, Kapfer R, Gruner SM (2005) High-pressure cooling of protein crystals without cryoprotectants. *Acta Crystallogr D Biol Crystallogr* 61(Pt 7):881–890.
20. Domsic JF, et al. (2008) Entrapment of carbon dioxide in the active site of carbonic anhydrase II. *J Biol Chem* 283(45):30766–30771.
21. Liang JY, Lipscomb WN (1990) Binding of substrate CO₂ to the active site of human carbonic anhydrase II: A molecular dynamics study. *Proc Natl Acad Sci USA* 87(10): 3675–3679.
22. Fisher SZ, et al. (2007) Atomic crystal and molecular dynamics simulation structures of human carbonic anhydrase II: Insights into the proton transfer mechanism. *Biochemistry* 46(11):2930–2937.
23. Maupin CM, Voth GA (2007) Preferred orientations of His64 in human carbonic anhydrase II. *Biochemistry* 46(11):2938–2947.
24. Supuran CT (2008) Carbonic anhydrases: Novel therapeutic applications for inhibitors and activators. *Nat Rev Drug Discov* 7(2):168–181.
25. Temperini C, Scozzafava A, Vullo D, Supuran CT (2006) Carbonic anhydrase activators. Activation of isozymes I, II, IV, VA, VII, and XIV with L- and D-histidine and crystallographic analysis of their adducts with isoform II: Engineering proton-transfer processes within the active site of an enzyme. *Chemistry* 12(27):7057–7066.
26. Briganti F, et al. (1997) Carbonic anhydrase activators: X-ray crystallographic and spectroscopic investigations for the interaction of isozymes I and II with histamine. *Biochemistry* 36(34):10384–10392.
27. Briganti F, et al. (1998) A ternary complex of carbonic anhydrase: X-ray crystallographic structure of the adduct of human carbonic anhydrase II with the activator phenylalanine and the inhibitor azide. *Inorg Chim Acta* 275-276:295–300.
28. Temperini C, Scozzafava A, Puccetti L, Supuran CT (2005) Carbonic anhydrase activators: X-ray crystal structure of the adduct of human isozyme II with L-histidine as a platform for the design of stronger activators. *Bioorg Med Chem Lett* 15(23): 5136–5141.
29. Temperini C, Scozzafava A, Vullo D, Supuran CT (2006) Carbonic anhydrase activators. Activation of isoforms I, II, IV, VA, VII, and XIV with L- and D-phenylalanine and crystallographic analysis of their adducts with isozyme II: Stereospecific recognition within the active site of an enzyme and its consequences for the drug design. *J Med Chem* 49(10):3019–3027.
30. Silverman DN, Tu CK, Lindskog S, Wynns GC (1979) Rate of exchange of water from the active-site of human carbonic anhydrase-C. *J Am Chem Soc* 101(22):6734–6740.
31. Riccardi D, et al. (2006) “Proton holes” in long-range proton transfer reactions in solution and enzymes: A theoretical analysis. *J Am Chem Soc* 128(50):16302–16311.
32. Roy A, Taraphder S (2007) Identification of proton-transfer pathways in human carbonic anhydrase II. *J Phys Chem B* 111(35):10563–10576.
33. Khalifah RG, Strader DJ, Bryant SH, Gibson SM (1977) Carbon-13 nuclear magnetic resonance probe of active-site ionizations in human carbonic anhydrase B. *Biochemistry* 16(10):2241–2247.
34. Forsman C, Behravan G, Osterman A, Jonsson BH (1988) Production of active human carbonic anhydrase II in *E. coli*. *Acta Chem Scand B* 42(5):314–318.
35. Håkansson K, Carlsson M, Svensson LA, Liljas A (1992) Structure of native and apo carbonic anhydrase II and structure of some of its anion-ligand complexes. *J Mol Biol* 227(4):1192–1204.
36. Kim CU, Hao Q, Gruner SM (2006) Solution of protein crystallographic structures by high-pressure cryocooling and noble-gas phasing. *Acta Crystallogr D Biol Crystallogr* 62(Pt 7):687–694.
37. McPherson A (1982) *The Preparation and Analysis of Protein Crystals* (Wiley, New York).
38. Henderson R (1990) Cryoprotection of protein crystals against radiation damage in electron and X-ray diffraction. *Proc Biol Sci* 241(1300):6–8.
39. Otwinowski Z, Minor W (1997) Processing of X-ray diffraction data collected in oscillation mode. *Methods Enzymol* 276:307–326.
40. Collaborative Computational Project, Number 4 (1994) The CCP4 suite: Programs for protein crystallography. *Acta Crystallogr D Biol Crystallogr* 50(Pt 5):760–763.
41. Murshudov GN, Vagin AA, Dodson EJ (1997) Refinement of macromolecular structures by the maximum-likelihood method. *Acta Crystallogr D Biol Crystallogr* 53(Pt 3): 240–255.
42. Perrakis A, Morris R, Lamzin VS (1999) Automated protein model building combined with iterative structure refinement. *Nat Struct Biol* 6(5):458–463.
43. Emsley P, Cowtan K (2004) Coot: Model-building tools for molecular graphics. *Acta Crystallogr D Biol Crystallogr* 60(Pt 12 Pt 1):2126–2132.